Constrained Synthesis and Organization of Catalytically Active Metal Nanoparticles by Self-Assembled Protein Templates

By *Silke Behrens,* Arnon Heyman, Robert Maul, Sarah Essig, Sebastian Steigerwald, Aina Quintilla, Wolfgang Wenzel, Jochen Bürck, Or Dgany,* and *Oded Shoseyov**

Recently, there has been great interest in self assembled biostructures as a tool for the controlled fabrication of one , two , or three dimensional ordered nanomaterials and devices.[1] Numerous proteins self assemble into well defined superstruc tures (sheets, wires, tubes, or capsids) and have been used to template particle arrays and nanowires of inorganic materials,[2] providing unique inorganic biomolecule hybrids with properties derived from both the inorganic (of magnetic, electric, or optical nature) and the biological (specific recognition capabilities) material. One problem often encountered in protein based biotemplating techniques, however, is the sensitivity of proteins to the ''unnatural'' reaction conditions, for example, towards variation of the pH, higher temperatures (>37 °C), and the presence of non native chemicals. Stress related proteins may overcome these difficulties because of their robustness and tolerance of a variety of unnatural conditions.[3] Moreover, their potential for application has just recently been demonstrated for Flash memory device fabrication based on chaperonin derived nanocrystal assemblies.[4]

We report here the size constrained synthesis of catalytically active metal particles using a genetically modified stable protein (SP1) expressed during droughts in aspen plants (*populus tremula*).[5] SP1 is a ring shaped homododecamer (12 mer), 11 nm in diameter, with a central, 2 3 nm inner pore and a width of 4 5 nm. The protein has an extremely high thermal and chemical stability, for example, it exhibits a melting temperature of 107 °C and resistance to detergents, such as sodium dodecyl sulfate (SDS), and to proteases.[6] We have genetically fused a histidine tag to the N terminus of SP1 (6hisSP1), thus obtaining a variant with 72 additional His residues facing the inner pore of the ring structure.[7] Histidine is a typical metal binding site in proteins due to the presence of the deprotonated N3 atom in the imidazole ring, analogous to the N7 atom of guanine or adenine.[8,9]

When the 6hisSP1 mutant was treated with Na_2PdCl_4 (typically 720 Pd atoms per dodecamer) for 2 h at room temperature, a homogenous pale yellow solution resulted. Excess Pd was removed by dialysis. The Pd^{2+} ions were subsequently reduced by a reduction bath containing dimethylamine borane (DMAB), resulting in a clear brown colloidal solution, which was stable for several months (see Supporting Information). Under the same conditions, a black precipitate was formed in protein free experiments. When the reduction was performed under the same conditions in the presence of the wild type SP1 protein (w.t. SP1), which has no histidine, black aggregates precipitated out of solution after between 1 h and one day, indicating that the histidine in the protein inner pore of 6hisSP1 initiates the desired reaction. Transmission electron microscopy (TEM) imaging of the precipitate revealed aggregated, 3.4 nm sized particles (see Supporting Information). The particulate texture and size suggest that the wild type template also influences initial particle nucleation. However, binding of the particles to the protein seems to be weak, and the particles, once formed, are released and precipitate from the solution.

The initial UV vis spectrum revealed two very small shoulders, corresponding to tryptophanes and tyrosines at 280 nm and 290 nm and to the palladium/protein complex at 340 nm, respectively (Fig. 1A). After reduction, the solution spectrum changed significantly, with an increase in the absorbance from the ultraviolet to the visible region, suggesting that the band structure of the Pd nanoparticles was formed (Fig. 1A). An increase of absorption in this range has been reported for Pd(0) nanoparticles by the polyol method.[10]

SDS polyacrylamide gel electrophoresis (PAGE) analysis of Pd 6hisSP1 after reduction, demonstrated that the protein

[*] Dr. S. Behrens, S. Essig, and S. Steigerwald
Institute of Technical Chemistry
Forschungszentrum Karlsruhe
76021 Karlsruhe (Germany)
E mail: silke.behrens@itc cpv.fzk.de
Prof. O. Shoseyov, A. Heyman, Dr. O. Dgany
Robert H. Smith Institute of Plant Science and Genetics
Hebrew University
Rehovot (Israel)
E mail: shoseyov@agri.huji.ac.il
R. Maul, Dr. A. Quintilla, Dr. W. Wenzel
Institute of Nanotechnology
Forschungszentrum Karlsruhe
76021 Karlsruhe (Germany)
Dr. A. Quintilla, Dr. W. Wenzel
DFG Center for Functional Nanostructures
Wolfgang Gaede Str. 1
76131 Karlsruhe (Germany)
Dr. J. Bürck
Institute for Biological Interfaces
Forschungszentrum Karlsruhe
76021 Karlsruhe (Germany)

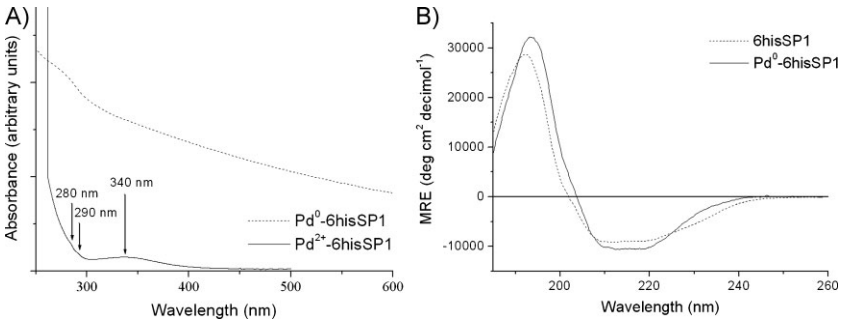

Figure 1. UV vis absorption and CD spectra of Pd 6hisSP1. A) UV vis absorption spectra of the protein bound Pd^{2+} complex before reduction (Pd^{2+} 6hisSP1) and the Pd^{0} 6hisSP1 nanobio conjugates after reduction (diluted 1:10). B) CD spectra of 6hisSP1 and Pd^{0} 6hisSP1 (shown as mean residue ellipticity, MRE).

maintained its original characteristics and the dodecameric structure as expected, and can be denatured only when boiled in the presence of SDS (see Supporting Information). 6hisSP1 appears at 13 kDa as monomer when boiled with SDS and at ≈130 kDa when not boiled prior to run.

The Pd 6hisSP1 conjugate was analyzed using gel filtration fast protein liquid chromatography (FPLC). A high molecular weight peak was eluted at the column void volume (higher than 669 kDa, see Supporting Information). These high molecular weight eluted fractions were further analyzed with SDS PAGE and revealed the 6hisSP1 monomer. The monomer appearance in the high molecular weight fractions indicated the formation of large conjugate structures as a result of the Pd reduction in the protein inner pore.

The Pd 6hisSP1 conjugate complex was further imaged by TEM. Figure 2A D shows the chain formation of Pd 6hisSP1. Pd particles imbedded in the inner pore of the protein serve as connectors between adjacent 6hisSP1's, thus forming large defined structures. The TEM images of unstained samples clearly show that the metal clusters are almost monodisperse particles, and their shape is roughly spherical (Fig. 2E). The particle diameter was determined to be (2.85 ± 0.5) nm, as shown in the histogram in Figure 2F. Additional structural characterization was performed using high resolution TEM (HRTEM), which manifests distinctly visible lattice fringes indicative of crystalline order and the metallic character of the particles. The measured interplanar spacing is 0.227 nm for most of the particles, which is in good agreement with the (111) lattice d spacing of bulk face centered cubic palladium with a unit cell size of 0.39 nm. In addition, the purity of the deposited Pd particles was verified by energy dispersive X ray analysis (EDX, Fig. 2F). The palladium and protein content of the Pd 6hisSP1 product was determined by inductively coupled plasma atomic emission spectroscopy (ICP AES) and UV absorbance at 280 nm, respectively, resulting in 624 Pd atoms per 6hisSP1 oligomer on average. Our results from ICP AES, UV spectrometry (624 Pd atoms/oligomer), and TEM measurements (see Fig. 2F for particle size distribution) agree well with a particle radius of about 2.8 nm, which would be expected on the basis of closed sphere packing and magic numbers for five shell clusters of 561 Pd atoms. These observations suggest that not only the position of the Pd particles but also particle growth was controlled by the protein template. TEM images suggest that size constrained particle nucleation was preferentially per formed in the central, 2 3 nm sized pore. Once a Pd particle is formed, it may further serve as a linker to create metal nanoparticle protein chains. TEM images of the stained Pd 6hisSP1 composite material reveal regular Pd nanoparticle 6hisSP1 chains. Such chain like structures spontaneously self assemble in the solution. A mean center to center distance of (6.20 ± 1.13) and (6.32 ± 0.91) nm was measured for neighboring particles (from unstained TEM images) and proteins (from TEM images stained by uranyl acetate) in such chain like structures, respectively. By taking into account that the observed width depends on the preparation procedure for electron microscopy, that is, staining, drying, interaction with the TEM grid, and flattening on the grid, the observed distances are in agreement with the 4 5 nm width of the ring like SP1 structure, and suggest stacking of protein rings mediated by residual his tags and metal particles. Such a protein particle chain formation has previously been observed with Ni nitrilotriacetic acid (NTA) functionalized Au nanoparticles and 6hisSP1,[7] whereas 6hisSP1 alone does not typically assemble into chain like structures (see Supporting Information).

Circular dichroism (CD) spectroscopy was used to analyze the secondary structure of 6hisSP1 before and after the metallization procedure. Figure 1b compares the CD spectra of the 6hisSP1 mutant and the Pd 6hisSP1 nano bioconjugate. The 6hisSP1 mutant displays the typical CD bands of a protein that has a significant α helical fraction with a maximum around 192 nm and two minima at 208 and 221 nm, respectively. After metallization and binding of Pd nanoparticles to 6hisSP1, the maximum shifts somewhat to 193 nm, and the negative bands approach each other slightly, leading to a steeper shape of the ''trough'' between the minima. The mean residue ellipticities also show minor intensity changes. These features altogether indicate only small conforma tional changes. Thus, one can clearly state that the protein was not denatured during the metallization reaction. This is also reflected in the secondary structure analysis of the experimental CD spectra based on different estimation algorithms (see Table 1, Supporting Information). We observed a slight increase in α helix after the binding of the Pd particles, while for β strand, β turn, and unordered conformation no clear trend and only minor changes are obtained. In further investigations, we will investigate the dependence of the observed CD spectra as a function of the Pd/protein ratio during the metallization reaction.

To elucidate these findings, we employed a recently developed atomistic protocol for simulation of nanoscale structure forma tion on long time scales.[11] Our simulations comprise two parts: in the first part, we ''grow'' the nanoparticle, one atom at a time in molecular mechanics simulations. We observe the nucleation of several Pd nanocrystals emanating from the unprotonated side chain His N3 atoms (Fig. 3A), which coalesce into a single multidomain Pd nanoparticle that spans the entire pore (Fig. 3B). Using the generated nanoparticle/protein complex, we can analyze the fluctuations of the protein with and without nanoparticle in molecular dynamics simulations using the

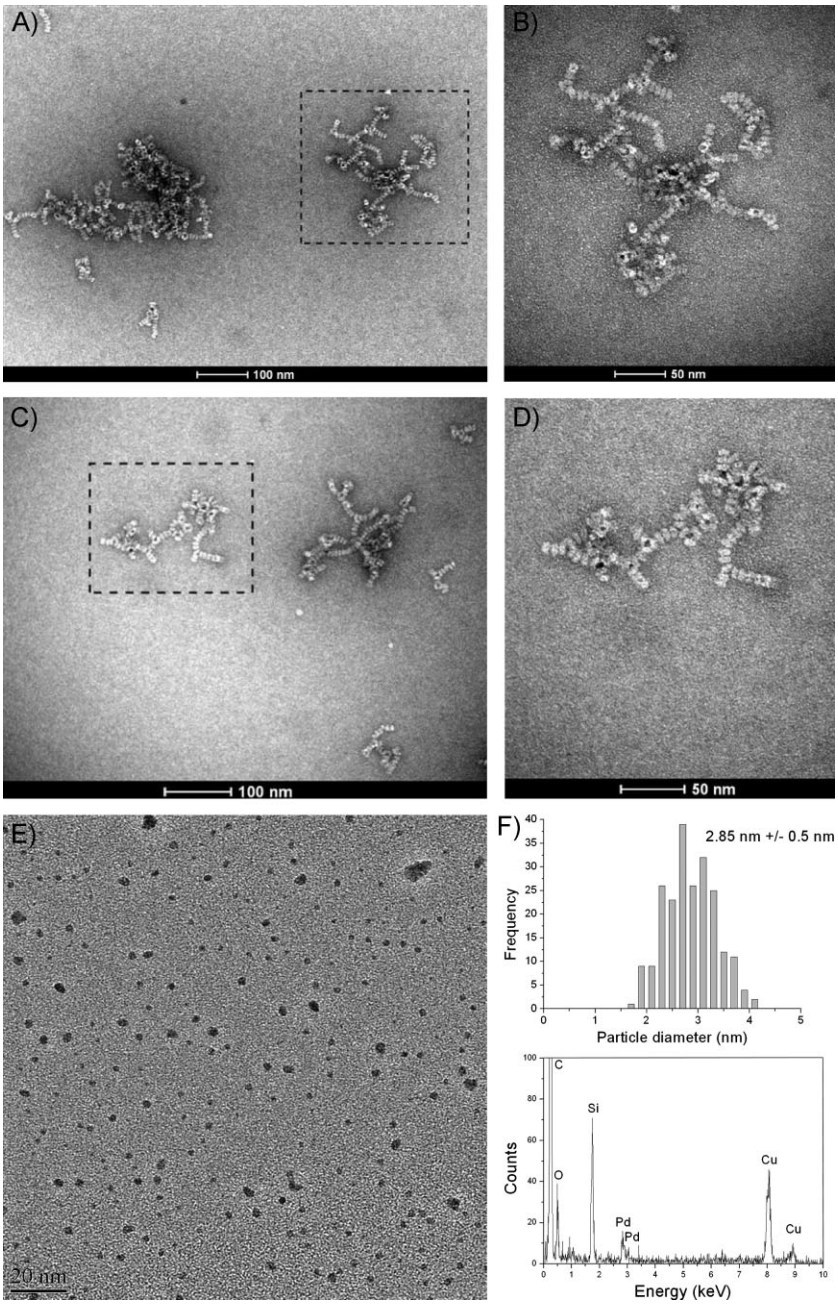

Figure 2. TEM images of Pd 6HisSP1 A D) negatively stained with uranyl acetate. B) and D) are magnifications of A) and C) respectively (the protein in white and the Pd nanoparticles in black). E) Unstained sample. F) Particle size distribution (mean particle diameter (2.85 ± 0.5) nm) and EDX spectrum of Pd 6hisSP1 (Cu originates from supporting TEM grid).

Assisted Model Building and Energy Refinement (AMBER)[12] forcefield. We find that the protein alone equilibrates into a conformational ensemble with approximately 2.5 Å RMSD (root mean square deviation) from the starting structure, and the presence of the metal nanoparticle constrains the conformational ensemble to within 1.1 Å RMSD of the starting conformation. In agreement with the experimental observations, the overall secondary structure content and tertiary arrangement is not influenced by the presence of the nanoparti cles. However, we find the structural fluctua tions of the protein in complex with the nanoparticles are reduced by approximately 28% (Fig. 3C), when compared to the fluctua tions of the protein alone. The observed reduction of fluctuations in the complex, akin to a reduced temperature, is commensurate with the observed increase in CD signal. The change in the CD signal can thus be under stood as a result of reduced fluctuations in the protein due to the constraints imposed by the presence of the nanoparticle, and not by an actual increase of helical content in the secondary structure.

To investigate the catalytic properties of Pd 6hisSP1, we chose the catalytic reduction of 4 nitrophenol (NP) by $NaBH_4$ to 4 amino phenol (AP) as a model reaction and monitored its kinetics by UV vis spectroscopy (Fig. 4). The peak at 400 nm is attributed to 4 nitrophenoate ions appearing immediately after addition of $NaBH_4$. After addition of the Pd nanoparticles, the peak at 400 nm decreases gradually, and a new peak, attributed to AP, appears at 300 nm. Since excess $NaBH_4$ was used, the BH_4^- concentration remained essentially constant throughout the reaction, so that the reduction rate was assumed as independent of the $NaBH_4$ concentration, and treated as pseudo first order in NP concentration. The ratio c_t/c_0 of the NP concentration at time t and 0 was obtained from the relative intensity of the respective absor bances A_t/A_0 at 400 nm (Fig. 4B). After mixing all reactants, a time lag was observed without change in absorbance, which was dependent on the applied catalyst concentration.[13] The linear relations of $\ln(c/c_0)$ were used to calculate the values of the apparent rate constant k_{app} (Fig. 4C). The rate constant increases linearly with the concentration of the Pd 6hisSP1 conjugate. The measured rate constant would thus allow in return quantifying the parti cle attached 6hisSP1 protein. These nanoparti cle 6hisSP1 composites can be further manipulated by genetic engineering to attach specific ligands or functional protein domains (as demonstrated before with SP1),[14] resulting in functionalized nanocatalysts. The catalytic properties of such biofunctional nanoparticle labels may be used for catalytic signal ampli fication in optical assays, providing a simple and ultrasensitive method for the detection and quantification of biomolecules in early stages of biomedical diagnosis.[15,16]

Our studies demonstrate that these stress related protein mutants are appealing templates for the synthesis of mono disperse metal particles of various natures, and the generated particles provide a mortar to construct novel geometrical architectures of hybrid nanoparticle protein complexes. The

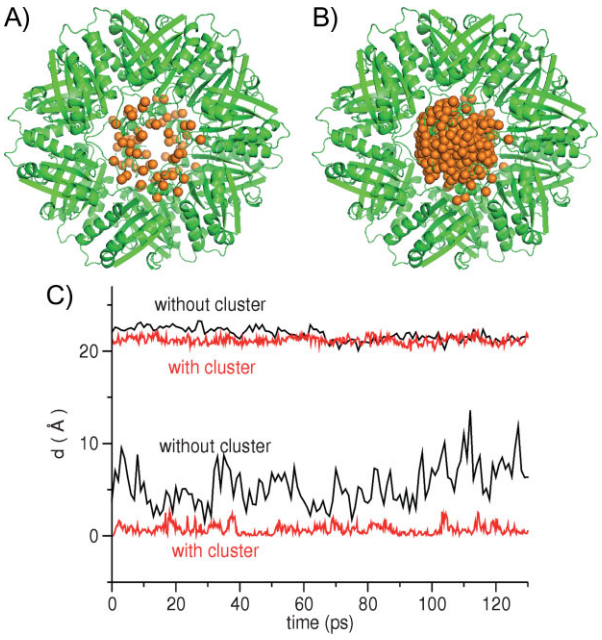

Figure 3. Intermediate (A: 90 atoms) and final (B: 800 atoms) structures of a nanoparticle in the deposition simulations. C) Fluctuation of a single C_α atom (in Gln 23, bottom curves) in a helical region and of the end to end distance of helix $C_\alpha^{Gln\ 23}$ $C_\alpha^{Leu\ 37}$ (top curves) in the MD trajectories with (red) and without (black) the nanoparticle. The nanoparticles induced reduction in the fluctuations explains the observed increase in the CD signal without a change in the fraction of helical content in the protein.

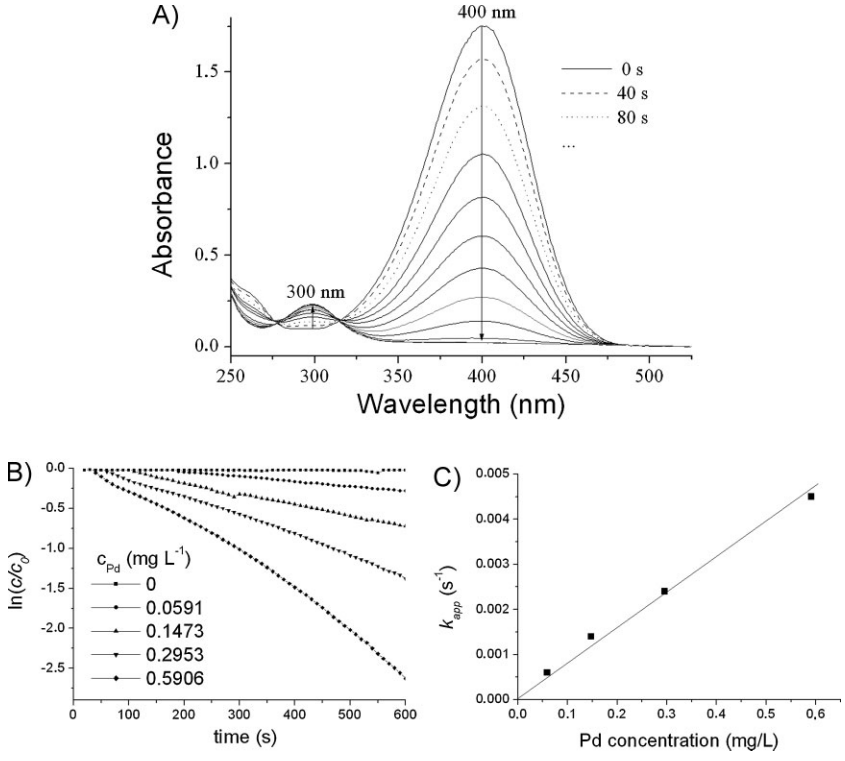

Figure 4. Catalytic performance. A) UV vis absorption spectra for the reduction of 4 nitrophenol catalyzed by Pd 6hisSP1. B) Influence of the Pd 6hisSP1 concentration on the reduction of 4 nitrophenol (4 nitrophenol 0.1 mmol L^{-1}, $NaBH_4$ 10.5 mmol L^{-1}, T 22 °C). C) Rate constant as a function of the Pd 6hisSP1 concentration (in mg Pd L^{-1}).

protein structure remained intact after particle deposition and, thus, may be further functionalized by genetic engineering with affinity reagents for site specific targeting. Moreover, Pd 6hisSP1 composites represent active biofunctional nanocatalysts, providing building blocks for future site specific nanocatalysts that would allow sensitivity enhancement in diagnostic assays by catalytic signal amplification. As shown in recent experiments in mice, w.t. SP1 accumulates in tumors and shows no significant immune response after repeated injection, indicating that it may indeed be used to target active nanoparticles to solid tumors for both imaging and therapy. Such biofunctional, protein nanoparticle hybrids will thus be interesting for diverse future applications, such as in biosensing, targeted reagent delivery, site specific tumor imaging, therapy, and biomedical diagnosis.

Experimental

All materials were purchased from Sigma Aldrich and used as received without further purification. Nanopure water (18.2 MΩ cm ^{1}), prepared with a Milli Q Plus water system, was used throughout the experiments.

Protein Expression and Purification: 6hisSP1 was expressed in *e.coli* bacteria strain BL21 and purified as described previously [7].

Synthesis of Pd Nanoparticles: In a typical procedure, 1 mL of a 6hisSP1 solution in piperazine diethanesulfonic acid (PIPES) buffer (protein concentration: 1.7 mg mL ^{1}) was treated with an equal volume of a Na_2PdCl_4 solution (8 mM in PIPES) for 2 h at room temperature and dialyzed against ten fold diluted PIPES buffer for 2 h. The solution was subsequently reduced by applying an equal volume of a reduction bath containing sodium citrate (25 g L ^{1}), lactic acid (25 g L ^{1}), and dimethylamine borane (DMAB, 2.5 g L ^{1}) at pH 6.8. The proportion of Pd to protein in the hybrids was determined by atomic emission spectroscopy (Varian Liberty 150) and UV vis spectrometry [17], respectively.

Gel Filtration FPLC: A prepacked SuperdexTM 200 10/300 GL column was obtained from Amersham Pharmacia Biotech (USA). The column was calibrated using a molecular weight markers kit, product no. MW GF 1000 (Sigma Aldrich, St. Louis, MO, USA). The column void volume was determined using blue dextran. Samples were loaded to the column using TBS buffer pH 7.4 as a loading buffer at a flow rate of 0.7 mL min ^{1}. The protein was detected using a UV detector at a wavelength of 280 nm. Samples were collected at the column exit every 0.5 min.

CD Spectroscopy: The CD spectra of 6hisSP1 and of the Pd 6hisSP1 colloidal solution (both in 10 mM phosphate buffer) were recorded using a J 815 spectropolarimeter (JASCO, Groß Umstadt, Germany) at 20 °C using a quartz glass cuvette with 0.1 cm path length. Prior to CD spectroscopy, the samples were dialyzed overnight against phosphate buffer (10 mM). The protein concentration of 6hisSP1 and Pd 6hisSP1 was determined based on the absorbance of the protein at 280 nm under denaturing conditions, according to the method described by Edelhoch [17].

Catalytic Reaction: 0.5 mL Pd 6hisSP1 of various concentrations were treated with 0.5 mL freshly prepared $NaBH_4$ solution (63 mM) for 15 min. 2 mL 4 nitrophenol (0.15 mM) was added, and the time dependent absorption spectra were recorded every 5 s from 250 550 nm at 22 °C.

Electron Microscopy: TEM data were collected using a FEI Tecnai F20 with field emission gun at 200 kV and equipped with an energy dispersive X ray (EDX) spectrometer. Typically, a 20 μL droplet of the sample was placed on a carbon coated 400 mesh copper grid, and the excess liquid was removed with filter paper. When negative staining was performed, the dried sample on the TEM grid was additionally exposed to a 1% uranyl acetate solution for ~1 min.

Simulation: In the deposition simulation, we started from the crystal structure of w.t. SP1 to which we attached six His tags at the experimental positions. We then deposited up to 1600 Pd ions, one atom at a time, using a kinetic Monte Carlo Method. In each simulation, the Pd ion is placed at a random position outside the protein and evolved for 30 000 steps in the electrostatic potential generated from the protein (AMBER charges) and the partially formed Pd cluster using also a short range Gupta potential [18] for Pd. When the Pd ion attaches to an existing cluster, it is reduced. Explicit water all atom molecular dinamycs (MD) simulations were performed in an 11 nm box with periodic boundary conditions in an NPT ensemble using the Nose Hoover thermostat. The systems were first energy minimized and equilibrated to 300 K/1 atm (1 atm 101 325 Pa) before the production runs of up to 4.5 ns were performed at the Computational Science Center of KIST, Seoul, Korea. The Pd cluster was held fixed in the MD simulations.

Acknowledgements

The authors acknowledge K. Niederer and I. Kondov for technical assistance. WW acknowledges financial support from the biomaterials program of the Landesstiftung Baden Württemberg, AQ from CFN project C5.1, and RM from DFG grant WE 1863/15 1. Supporting Information is available online from Wiley InterScience or from the author. S. B. and A. H. contributed equally to this paper.

[1] S. Behrens, *J. Mater. Chem.* **2008**, *18*, 3788.

[2] a) T. Ueno, M. Suzuki, T. Goto, T. Matsumoto, K. Nagayama, Y. Watanabe, *Angew. Chem. Int. Ed.* **2004**, *43*, 2527. b) S. Mark, M. Berkvist, X. Yang, L. Teixeira, P. Bhatnagar, E. Angert, C. Batt, *Langmuir* **2006**, *22*, 3763. c) S. Behrens, W. Habicht, K. Wagner, E. Unger, *Adv. Mater.* **2006**, *18*, 284. d) S. Behrens, J. Wu, W. Habicht, E. Unger, *Chem. Mater.* **2004**, *16*, 3085. e) S. Behrens, J. Wu, W. Habicht, E. Unger, *Surf. Interface Anal.* **2006**, *38*, 1014. f) R. Bekeredjian, S. Behrens, J. Ruef, E. Dinjus, E. Unger, M. Baum, H. F. Kuecherer, *Ultrasound in Med. & Biol.* **2002**, *28*, 691.

[3] a) M. Klem, D. Willits, D. Solis, A. Belcher, M. Young, T. Douglas, *Adv. Funct. Mater.* **2005**, *15*, 1489. b) R. McMillan, J. Howard, N. Zaluzec, H. Kagawa, R. Mogul, Y. F. Li, C. Paavola, J. Trent, *J. Am. Chem. Soc.* **2005**, *127*, 2800. c) Z. Varpness, J. Peters, M. Young, T. Douglas, *Nano Lett.* **2005**, *5*, 2306.

[4] S. Tang, C. Mao, Y. Liu, D. Kelly, S. Banerjee, *IEEE Trans. Electron Devices* **2007**, *54*, 433.

[5] a) W. X. Wang, D. Pelah, T. Alergand, O. Shoseyov, A. Altman, *Plant Physiol.* **2002**, *130*, 865. b) W. Wang, O. Dgany, O. Dym, A. Altman, O. Shoseyov, O. Almog, *Acta Crystallogr. Sect. D* **2003**, *59*, 512.

[6] O. Dgany, A. Gonzalez, O. Sofer, W. Wang, G. Zolotnitsky, A. Wolf, Y. Shoham, A. Altman, A. Wolf, O. Shoseyov, O. Almog, *J. Biol. Chem.* **2004**, *279*, 51516.

[7] I. Medalsy, O. Dgany, M. Sowwan, H. Cohen, A. Yukashevska, S. G. Wolf, A. Wolf, A. Koster, O. Almog, I. Marton, Y. Pouny, A. Altman, O. Shoseyov, D. Porath, *Nano Lett.* **2008**, *8*, 473.

[8] S. Behrens, K. Rahn, W. Habicht, K. J. Böhm, H. Rösner, E. Dinjus, E. Unger, *Adv. Mater.* **2002**, *14*, 1621.

[9] L. C. Ciacchi, M. Mertig, R. Seidel, W. Pompe, A. De Vito, *Nanotechnology* **2003**, *14*, 840.

[10] T. Teranishi, M. Miyake, *Chem. Mater.* **1998**, *10*, 594.

[11] J. J. Kwiatkowski, J. Nelson, H. Li, J.-L. Brédas, W. Wenzel, C. Lennartz, *PhysChemPhys* **2008**, *10*, 1852.

[12] A. Case, T. Darden, T. Cheatham, C. Simmerling, J. Wang, R. Duke, R. Luo, K. Merz, B. Wang, D. Pearlman, M. Crowley, S. Brozell, V. Tsui, H. Gohlke, J. Mongan, V. Hornak, G. Cui, P. Beroza, C. Schafmeister, J. Caldwell, W. Ross, P. Kollman, *Amber 8*, University of California, San Francisco **2004**.

[13] Y. Mei, G. Sharma, Y. Lu, M. Ballauff, *Langmuir* **2005**, *21*, 12229.

[14] a) A. Heyman, I. Levy, A. Altman, O. Shoseyov, *Nano Lett.* **2007**, *7*, 1575. b) A. Heyman, Y. Barak, J. Caspi, D. B. Wilson, A. Altman, E. A. Bayer, O. Shoseyov, *J. Biotechnol.* **2007**, *131*, 433.

[15] D. Georganopoulou, L. Chang, J. Nam, C. Thaxton, E. Mufson, W. Klein, C. Mirkin, *Proc. Natl. Acad. Sci. USA* **2005**, *102*, 2273.

[16] J. Das, M. A. Aziz, H. Yang, *J. Am. Chem. Soc.* **2006**, *128*, 16022.

[17] H. Edelhoch, *Biochemistry* **1967**, *6*, 1948.

[18] X. Shao, X. Liu, W. Cai, *J. Chem. Theor. Comput.* **2005**, *1*, 762.